J Biomol NMR (2009) 43:161–170
DOI 10.1007/s10858-009-9299-x

ARTICLE

Improved accuracy of ^{15}N–^{1}H scalar and residual dipolar couplings from gradient-enhanced IPAP-HSQC experiments on protonated proteins

Lishan Yao · Jinfa Ying · Ad Bax

Received: 22 November 2008 / Accepted: 7 January 2009 / Published online: 10 February 2009

Abstract The presence of dipole-dipole cross-correlated relaxation as well as unresolved E.COSY effects adversely impacts the accuracy of $^{1}J_{NH}$ splittings measured from gradient-enhanced IPAP-HSQC spectra. For isotropic samples, the size of the systematic errors caused by these effects depends on the values of $^{2}J_{NH\alpha}$, $^{3}J_{NH\beta}$ and $^{3}J_{HNH\alpha}$. Insertion of band-selective ^{1}H decoupling pulses in the IPAP-HSQC experiment eliminates these systematic errors and for the protein GB3 yields $^{1}J_{NH}$ splittings that agree to within a root-mean-square difference of 0.04 Hz with values measured for perdeuterated GB3. Accuracy of the method is also highlighted by a good fit to the GB3 structure of the ^{1}H-^{15}N RDCs extracted from the minute differences in $^{1}J_{NH}$ splitting measured at 500 and 750 MHz ^{1}H frequencies, resulting from magnetic susceptibility anisotropy. A nearly complete set of $^{2}J_{NH\alpha}$ couplings was measured in GB3 in order to evaluate whether the impact of cross-correlated relaxation is dominated by the ^{15}N–$^{1}H^{\alpha}$ or ^{15}N–$^{1}H^{\beta}$ dipolar interaction. As expected, we find that $^{2}J_{NH\alpha} \leq 2$ Hz, with values in the α-helix (0.86 ± 0.52 Hz) slightly larger than in β-sheet (0.66 ± 0.26 Hz). Results indicate that under isotropic conditions, N–H^{N}/N–H^{β} cross-correlated relaxation often dominates. Unresolved E.COSY effects under isotropic conditions involve $^{3}J_{HNH\alpha}$ and $J_{NH\alpha}$, but when weakly aligned any aliphatic proton proximate to both N and H^{N} can contribute.

Keywords Cross-correlated relaxation · GB3 · IPAP · Liquid crystal · Magnetic susceptibility anisotropy

Abbreviation
RDC residual dipolar coupling

Introduction

Measurement of residual dipolar couplings (RDCs) in proteins by solution state NMR provides an important source of structural information (Prestegard et al. 2000). Not only can the orientational information derived from such measurements be of very high precision, defining the orientation of vectors for a rigid molecule to within a few degrees, the common axis system relative to which the vectors are aligned provides a common reference frame for all vectors within the molecule. This sets RDCs apart from restraints derived from NOEs and ^{3}J couplings, which define positions and torsion angles relative to neighboring atoms (Tolman et al. 1995; Tjandra et al. 1997). When RDCs are measured under linearly independent alignment orientations—up to five mutually orthogonal alignments in principle are accessible—inconsistencies between the measurements and a rigid protein structure can provide quantitative information on the amplitude and direction of the internal dynamics of the corresponding internuclear vectors relative to the molecular frame (Peti et al. 2002; Tolman 2002; Bruschweiler 2003; Hus et al. 2003; Bouvignies et al. 2005; Bouvignies et al. 2006; Lakomek et al. 2006; Tolman and Ruan 2006; Lakomek et al. 2008; Lange et al. 2008; Yao et al. 2008b). If amplitudes of fluctuations

Electronic supplementary material The online version of this article (doi:10.1007/s10858-009-9299-x) contains supplementary material, which is available to authorized users.

L. Yao · J. Ying · A. Bax (✉)
Laboratory of Chemical Physics, NIDDK, National Institutes of Health, Bethesda, MD 20892-0520, USA
e-mail: bax@nih.gov

of the bond vector orientations are small, the impact of such dynamics on the measured RDCs is a small, second order perturbation. It reaches a maximum when the vector is oriented parallel to the z axis of the alignment tensor, and even then, random isotropic motion in a cone of semi-angle 7° reduces the motionally averaged RDC by only 1% relative to a static vector along that z axis. For quantitative analysis of RDCs in terms of internal motion, high accuracy of the RDC measurement is therefore of the utmost importance. Even though the reliability of a given RDC measurement is often estimated from the reproducibility of results in duplicate identical experiments, which can be extremely good, this type of random measurement error does not account for potential systematic errors inherent to the measurement itself (Cutting et al. 2002). In particular, the effect of cross-correlated relaxation, which can impact the relative contribution of unresolved multiplet components to the observed signal, has previously been identified as a potential source of systematic error in the measurement of scalar and dipolar couplings (Ottiger et al. 1998b; de Alba and Tjandra 2006a; de Alba and Tjandra 2006b).

Here, we describe a modified version of the gradient-enhanced ^{15}N–^{1}H IPAP-HSQC experiment, commonly used for ^{15}N–^{1}H RDCs in proteins, in which the effect of dipole-dipole cross-correlated relaxation is effectively removed. The modified experiment includes band-selective ^{1}H pulses that decouple the aliphatic protons from the amide ^{15}N nuclei. This modification removes the impact of dipole-dipole cross-correlated relaxation on the line shape and also removes small asymmetries in the line shapes of the ^{15}N–^{1}H correlations that can result from E.COSY-type effects (Griesinger et al. 1986; Montelione and Wagner 1989) when aliphatic protons are scalar—and/or dipolar coupled to both the amide $^{1}H^{N}$ and ^{15}N.

We demonstrate that for the small protein GB3, measurement of ^{15}N–^{1}H $^{1}J_{NH}$ couplings with the band-selective decoupled (BSD) IPAP-HSQC experiment yields values that are within the random measurement error (0.04 Hz) from values recorded for a perdeuterated sample, where the cross-correlation and E.COSY effects are absent. Measurement of the magnetic field dependence of the ^{15}N–^{1}H $^{1}J_{NH}$ splittings, which include minute dipolar coupling contributions resulting from very weak protein alignment caused by magnetic susceptibility anisotropy of the protein (Gayathri et al. 1982; Tolman et al. 1995; Tjandra et al. 1996), as well as a small dynamic frequency shift (Tjandra et al. 1996; Werbelow 1996; de Alba and Tjandra 2006a; de Alba and Tjandra 2006b), yields results that fit well to the protein structure. Similarly, measurement of RDCs in the presence of liquid crystalline Pf1 yields values that fit very closely to vector orientations recently derived from measurements in a fully deuterated form of the protein (Yao et al. 2008b).

Experimental section

Sample expression and purification

K4AK19EV42E and K19AV42ED47K mutants of the 56-residue third IgG-binding domain of protein G, GB3, were made by expression in *Escherichia coli* BL21 (DE3*) cells, transformed with a pET-11 vector containing the mutated GB3 gene. Preparations were grown in M9 minimal media, containing $^{15}NH_4Cl$ and uniformly ^{13}C– enriched glucose as well as under conditions of full deuteration of the non-exchangeable protons, by expression in 99% D_2O, using M9 minimal media, containing uniformly $^{13}C/^{2}H$– enriched glucose (3 g/L) as well a 1 g/L $^{2}H/^{15}N/^{13}C$ Celtone growth medium (Martek Biosciences, Columbia, MD). Protein expression was induced by 0.2 mM IPTG. Cultures were centrifuged and resuspended in 20 ml PBS buffer. The cells were lysed at 80°C and centrifuged again. The supernatant was loaded on a Superdex 75 HiLoad 26/60 (Amersham Biosciences) column, equilibrated with NMR buffer (25 mM sodium phosphate, 50 mM NaCl, 0.05% w/v NaN_3, pH 6.5). Final K4AK19EV42E-GB3 NMR samples contained *ca* 4 mM $^{13}C/^{15}N$- or $^{15}N/^{13}C/^{2}H$-enriched protein in 300 µl volume (95%/5% H_2O/D_2O). A similar sample of the K19AV42ED47K $^{13}C/^{15}N$-GB3 was prepared that additionally included $\sim$ 8 mg/mL Pf1 phage (http://www.asla-biotech.com), yielding a solvent quadrupolar ^{2}H splitting of $\sim$ 7 Hz (Hansen et al. 1998).

NMR spectroscopy

All NMR experiments were carried out at 298 K on a Bruker Avance 750 MHz spectrometer, equipped with a three-axes gradient, triple resonance, room temperature probe, or on Bruker Avance 500 and 600 MHz spectrometers, equipped with z-axis gradient, triple resonance, cryogenic probes.

The 3D HNCA[HA]-E.COSY experiment for measurement of $^{2}J_{NH\alpha}$ (Wagner et al. 1991; Wang and Bax 1996) was recorded at 600 MHz, using high resolution in the ^{15}N dimension by extensive folding in this dimension and using mixed-time evolution (Ying et al. 2007), and a data matrix consisting of $75(t_1,\ ^{13}C^{\alpha}) \times 90(t_2,\ ^{15}N) \times 750(t_3,\ ^{1}H)$ complex points, $t_{1max} = 24.9$ ms, $t_{2max} = 86.4$ ms, $t_{3max} = 78$ ms, an interscan delay of 1.4 s, and 4 scans per FID. The time domain data were apodized with a squared, 90°-shifted sine bell function in the t_3 dimension and with regular 90°-shifted sine bell functions in both of the indirect dimensions, and zero-filled to $512 \times 512 \times 2048$ complex points. The refocusing INEPT and its $^{1}H^{N}$–selective sinc-shaped and Q3 pulses, used by Wang and Bax (1996), were replaced by Rance-Kay gradient-enhanced detection (Kay et al. 1992).

Measurement of $^{1}J_{HN}$ splittings was carried out with the ^{15}N-^{1}H IPAP-HSQC experiment of Fig. 3, either in the absence or presence of aliphatic ^{1}H decoupling during the t_1 evolution period. The selective aliphatic ^{1}H decoupling pulses are of the 180° IBURP type (Geen and Freeman 1991), centered at 2.4 ppm and covering a bandwidth of ± 2.8 ppm (pulse duration 1.6 ms at 500 MHz, 1.066 ms at 750 MHz). More details are given in the legend to Fig. 3.

Two-dimensional spectra were recorded as interleaved in-phase and anti-phase data matrices of 200(t_1) × 704(t_2) complex points each, $t_{1max} = 76$ ms, $t_{2max} = 70$ ms, an interscan delay of 1.5 s, and 2 scans per FID. The time domain data were apodized with a squared, 90°-shifted sine bell function in the t_2 dimension and with a 90°-shifted sine bell function in the t_1 dimension, and zero-filled to 4096 × 8192 complex points prior to 2D Fourier transformation. All spectra were processed and analyzed using the software package NMRPipe (Delaglio et al. 1995). Peak positions were determined by parabolic interpolation.

Results and discussion

Origins of systematic errors in $^{1}J_{NH}$ splitting measurement

As has been pointed out previously (Ottiger et al. 1998b; de Alba and Tjandra 2006a; de Alba and Tjandra 2006b), relaxation interference between the one-bond ^{15}N–^{1}H dipolar interaction and the dipolar coupling between ^{15}N and another nearby proton, H^{R}, causes the four components of the ^{15}N doublet-of-doublets to relax at different rates. Even while the $J_{N–HR}$ couplings are generally unresolved, their presence results in a small asymmetry of the line shape in the ^{15}N dimension, which impacts peak picking and thereby the accuracy of the $^{1}J_{NH}$ splitting (Fig. 1a, b).

A requirement for dipole-dipole cross-correlated relaxation to affect the measured $^{1}J_{NH}$ splittings is that the ^{15}N nucleus has a scalar or residual dipolar coupling to a remote proton H^{R}. For a non-zero coupling between ^{15}N and ^{1}H^{R}, the ^{15}N multiplet for this three-spin system is a doublet of doublets where, under the assumption of isotropic tumbling and ignoring both ^{15}N chemical shift anisotropy and internal dynamics, the multiplet components relax at rates proportional to $[1/r_{NH}^{6} \pm 2P_2(\cos\theta)/r_{NH}^{3} r_{N–HR}^{3} + 1/r_{N–HR}^{6}]$, where r_{NH} and $r_{N–HR}$ are the N–H bond length and the N–H^{R} internuclear distance, respectively, and $P_2(\cos\theta) = (3\cos^2\theta - 1)/2$, with θ the angle between the ^{15}N–^{1}H^{N} and ^{15}N–^{1}H^{R} vectors. For the case where $^{1}J_{NH}$ and $J_{N–HR}$ have the same sign, the plus sign in front of the $2P_2(\cos\theta)$ term refers to the outer and the minus sign to the inner multiplet components (Fig. 1a). The impact of cross-correlated relaxation on the coupling measurement depends not only on $P_2(\cos\theta)/r_{N–HR}^{3}$, but also on the size of the scalar or RDC interaction between the ^{1}H^{R} and ^{15}N nuclei (Fig. 1b). Three-bond J couplings between ^{15}N and ^{1}H$^{\beta}$, $^{3}J_{NH\beta}$, can be as large as 4 Hz and intraresidue H$^{\beta}$ nuclei also can be proximate to ^{15}N, depending on the backbone and sidechain torsion angles φ and χ_1. Indeed, dipole-dipole cross-correlated relaxation involving H$^{\beta}$ spins previously has been implicated as a source of error when extracting $^{1}J_{NH}$ splittings from intensity-modulated HSQC spectra by quantitative-J experiments (Tjandra and Bax 1997; de Alba and Tjandra 2006a; de Alba and Tjandra 2006b). For geometric reasons, the intraresidue distance, $r_{N-H\beta} \geq 2.3$Å, and $0 > P_2(\cos\theta) > -0.5$ when $r_{N-H\beta}$ is short. For the case where the intraresidue H$^{\alpha}$ is the passive spin, $r_{N-H\alpha} \approx 2.0$ Å and $P_2(\cos\theta)$ can be as large as + 0.6. So, even while the $^{2}J_{NH\alpha}$ couplings are known to be small (Bystrov 1976; Archer et al. 1991), their impact may be amplified by the short $r_{N-H\alpha}$ distance and the potentially large $P_2(\cos\theta)$ values. Contamination of the $^{1}J_{NH}$ splitting measurement resulting from intraresidue ^{1}H$^{\alpha}$–^{15}N interaction therefore is difficult to evaluate without a better estimate of the $^{2}J_{NH\alpha}$ coupling. Moreover, under conditions of weak alignment the two-bond ^{15}N–^{1}H$^{\alpha}$ RDC can become relatively large due to the short internuclear distance, thereby also impacting the magnitude of the distortion caused by cross-correlated relaxation. ^{15}N–H^{R} RDCs scale relative to the ^{15}N–^{1}H one-bond RDCs as $(r_{NH}/r_{N–HR})^{3}$, and are about 10-fold weaker than $^{1}D_{NH}$ couplings when assuming $r_{N–HR} = 2.2$ Å. For example, for a weakly aligned sample with axially symmetric alignment and $D_a \sim 10$–15 Hz, the largest ^{15}N–H^{R} RDCs are *ca* 2.0–3.0 Hz.

When ^{1}H^{R} has an RDC and/or scalar coupling to both the amide ^{15}N and ^{1}H^{N}, and the ^{1}H^{R} spin state is (partially) conserved between ^{15}N evolution and ^{1}H^{N} detection, the ^{1}H-^{15}N correlation will contain an E.COSY contribution (Griesinger et al. 1985; Griesinger et al. 1986; Meissner et al. 1998). Under isotropic conditions, only couplings to the intraresidue ^{1}H$^{\alpha}$ spin are sufficiently large to give rise to such an E.COSY pattern. However, under aligned conditions, any ^{1}H within ~ 3 Å from the ^{15}N nucleus can have a non-negligible RDC to both ^{15}N and ^{1}H^{N}. Although the magnitude of $^{3}J_{HNH\alpha}$ is tightly defined by the intervening backbone torsion angle, φ, very little quantitative information is available for the $^{2}J_{NH\alpha}$ coupling, except that these values are frequently too small to permit measurement from resonance intensities in quantitative-J (QJ) correlation experiments such as HNHB (Bystrov 1976; Archer et al. 1991). We therefore used an E.COSY-type experiment to measure the isotropic $^{2}J_{NH\alpha}$ couplings in GB3.

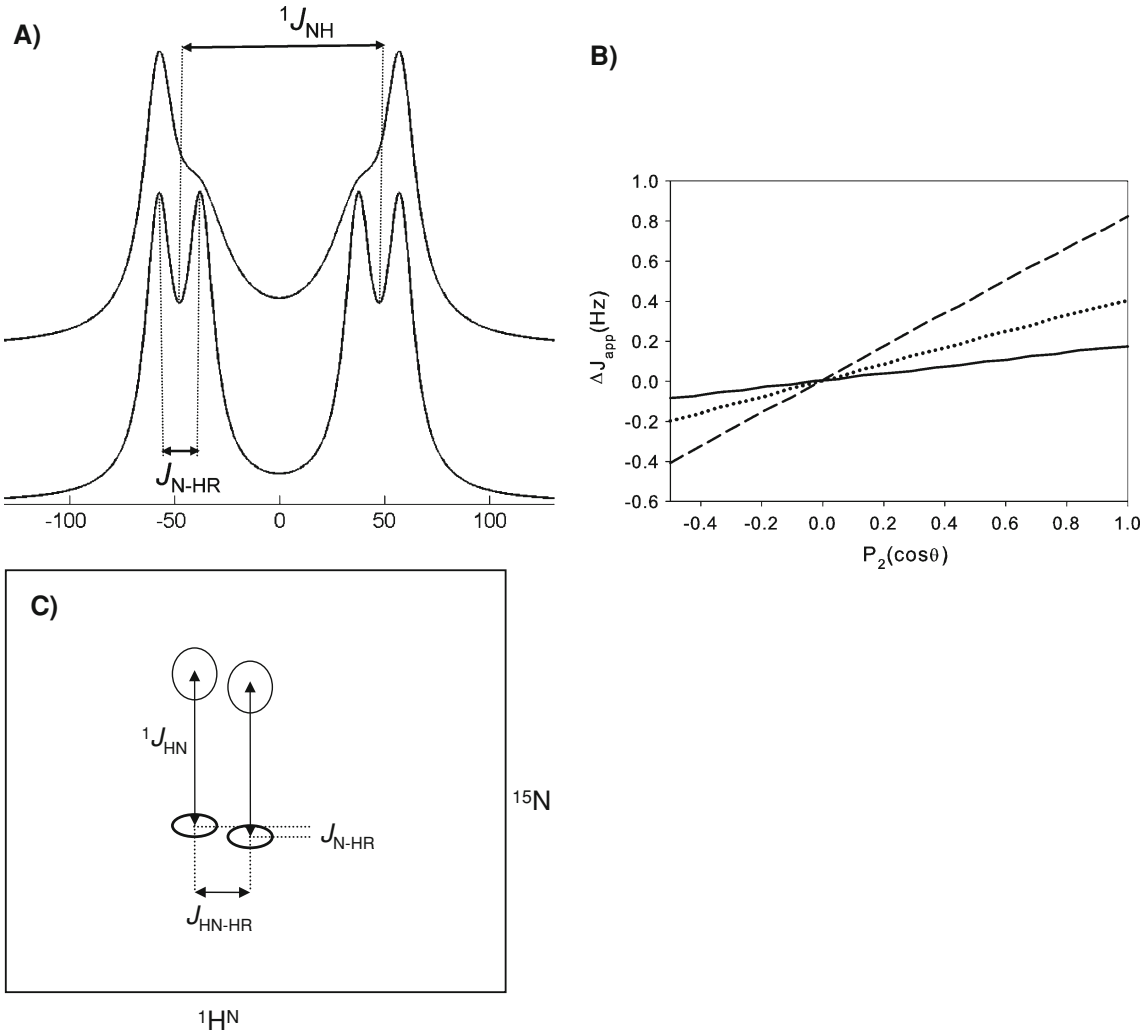

Fig. 1 The impact of a third spin, H^R, on the measurement of one-bond ^1H–^{15}N J splittings. (**a**) Interference between $^1H^R$–^{15}N and ^1H–^{15}N dipolar relaxation contributions cause differential line widths and amplitudes for the components of the ^{15}N multiplet. For visual purposes, a larger than realistic value is used for $J_{N–HR}$ (20 Hz). The lower multiplet is simulated in the absence of relaxation interference, with a line width of 15 Hz. The top spectrum corresponds to the case where $J_{N–HR}$ and $J_{N–H}$ have the same sign, and $P_2(\cos\theta) < 0$, with exaggerated relaxation interference and outer/inner line widths of 17/33 Hz. (**b**) Effect of the magnitude of the error in $^1J_{NH}$ splitting measurement ΔJ_{app}, calculated for $\tau_c = 10$ ns, $r_{NH} = 1.04$ Å, $r_{N–HR} = 2.5$ Å, ^{15}N CSA = 170 ppm, 600 MHz ^{1}H frequency, as a function of $P_2(\cos\theta)$, where θ is the H–N–H^R angle, in the absence of internal dynamics. Results are shown for three values of $J_{N–HR}$: 1.5 Hz (solid line), 3 Hz (dotted) and 4.5 Hz (dashed). The two extreme relaxation rates, corresponding to $P_2(\cos\theta) = 1$, are 13.9 ± 1.4 s^{-1}. The time domain data were apodized with an exponential function to yield a final linewidth of $\sim$12 Hz prior to peak picking. Splittings were determined from the distance between the highest points of the two ^{15}N–{$^1H^N$} doublet components. (**c**) Schematic diagram for the E.COSY character of ^1H–^{15}N HSQC correlations obtained with the gradient-enhanced $^{15}N \rightarrow {}^1H$ transfer scheme, with the passive spin H^R not being attached to ^{15}N. The appearance of the E.COSY effect is also impacted by the ^{15}N line width, shown larger for the upfield ^{15}N–{^1H} component than for the downfield one. Note that in practice the J_{HNHR} and $J_{N–HR}$ couplings are often not resolved, and the effect simply manifests itself as a skewed peak shape (see arrows in Fig. 4)

Conceptually the simplest way to avoid contamination of one-bond coupling measurements by the above mentioned relaxation interference or E.COSY effects utilizes perdeuteration of the protein, followed by back-exchange of the amide protons. Indeed, measurement of RDCs in a perdeuterated set of GB3 mutants recently has been shown to yield N–H vector orientations that yield exceptionally good Karplus curve fits (0.33 Hz rmsd) between H–N–C^α–H^α dihedral angles and experimental $^3J_{HNH\alpha}$ couplings (Yao et al. 2008a), and also results in RDC-derived N–H order parameters that closely follow the ^{15}N-relaxation-derived profile (Hall and Fushman 2003). As demonstrated in the present study, ^{1}H-^{15}N RDC measurements of comparable accuracy can be made in protonated proteins by suitable adaptation of the pulse sequence, including band-selective decoupling of the aliphatic protons.

Measurement of $^{2}J_{NH\alpha}$

For measurement of the $^{2}J_{NH\alpha}$ coupling we resort to the same type of HNCA[HA]-E.COSY experiment as was previously used for measurement of $^{3}J_{HNH\alpha}$ (Montelione and Wagner 1989; Wang and Bax 1996) (pulse scheme in Figure S1). However, as the E.COSY displacement is measured in the ^{15}N dimension of the spectrum, recording was optimized to obtain highest resolution in this dimension. In the 3D spectrum, two intraresidue ^{1}H-^{15}N-$^{13}C^{\alpha}$ correlations are obtained, corresponding to $^{1}H^{\alpha}$ in the $|\alpha>$ and $|\beta>$ spin states. The two correlations are separated in the $^{13}C^{\alpha}$ dimension by the large $^{1}J_{C\alpha H\alpha}$ splitting; their $^{2}J_{NH\alpha}$ displacement in the 3D spectrum can then easily be measured from the relative displacement of these two resonances in the ^{15}N dimension of the spectrum (Fig. 2a). Values as a function of residue number are shown in Fig. 2b, and confirm that $^{2}J_{NH\alpha}$ couplings indeed are very small ($\leq$1.6 Hz), with little dependence on residue type or secondary structure. For the intraresidue correlations in Fig. 2a, the downfield $^{13}C^{\alpha}$–{$^{1}H^{\alpha}$} doublet component connects with the upfield ^{15}N–{$^{1}H^{\alpha}$} component. Taking into account the negative sign of the ^{15}N and ^{13}C magnetogyric ratios, this indicates that $^{2}J_{NH\alpha}$ and $^{1}J_{C\alpha H\alpha}$ are of the same sign, and of opposite sign relative to the (negative) $^{1}J_{NH}$ couplings. The ^{15}N–{$^{13}C^{\alpha}$} de- and rephasing delays in the HNCA pulse scheme were adjusted to optimize sensitivity for the intraresidue connectivities, but weak correlations to the $^{13}C^{\alpha}$ of the preceding residue are also seen in Fig. 2a. For example, Fig. 2a shows the correlation between E24 H^{N} and A23 C^{α}. These weaker correlations also exhibit an E.COSY pattern, with the horizontal displacement corresponding to $^{3}J_{NH\alpha}$. Here, the downfield $^{13}C^{\alpha}$-{$^{1}H^{\alpha}$} doublet component correlates with the downfield ^{15}N-{$^{1}H^{\alpha}$} doublet component, indicating $^{1}J_{C\alpha H\alpha} \times {}^{3}J_{NH\alpha} < 0$, again taking into account the negative sign of γ_N. Values for $^{3}J_{NH\alpha}$ are largest (*ca*-1.6 Hz) when $\psi \approx -50°$, i.e., in α-helical conformations, and small (~ -0.5 Hz) for $\psi \approx 120°$ (β-sheet) (Wang and Bax 1995). However, with the sequential H^{α}–N distance being greater than 3 Å in α-helices, $^{3}J_{NH\alpha}$ contributions from cross-correlated relaxation to the perturbation of the apparent $^{1}J_{NH}$ splitting are negligible.

Band-selective-decoupled gradient-enhanced ^{15}N–^{1}H IPAP-HSQC

The ^{15}N–^{1}H IPAP-HSQC of Fig. 3 is conceptually very similar to the earlier version of this experiment (Ottiger et al. 1998a), which records two ^{15}N–^{1}H HSQC spectra in an interleaved manner without ^{1}H decoupling in the ^{15}N dimension. In one such spectrum, the ^{15}N–{^{1}H} doublet is in-phase; the other one is recorded with a delay of duration of $\sim (2\,{}^{1}J_{NH})^{-1}$, during which $^{1}J_{NH}$ is active, preceding t_1 evolution and causes the ^{15}N–{^{1}H} doublet to be antiphase. Due to the additional delay, this second spectrum is slightly weaker than the first one but, after applying a suitable scaling factor, addition or subtraction of the two spectra yields a spectrum containing either the downfield or the upfield ^{15}N–{^{1}H} multiplet component (Yang and Nagayama 1996). The scaling factor is 0.95 for GB3 system in our measurement, and becomes smaller as the rotational correlation time of the protein increases. Uniform scaling is adequate for GB3 and other proteins with uniform dynamics, but may be inadequate for systems with variable dynamic properties, e.g., when the protein contains long flexible loops. The problem can be partially solved by reducing the relaxation differences between IP and AP

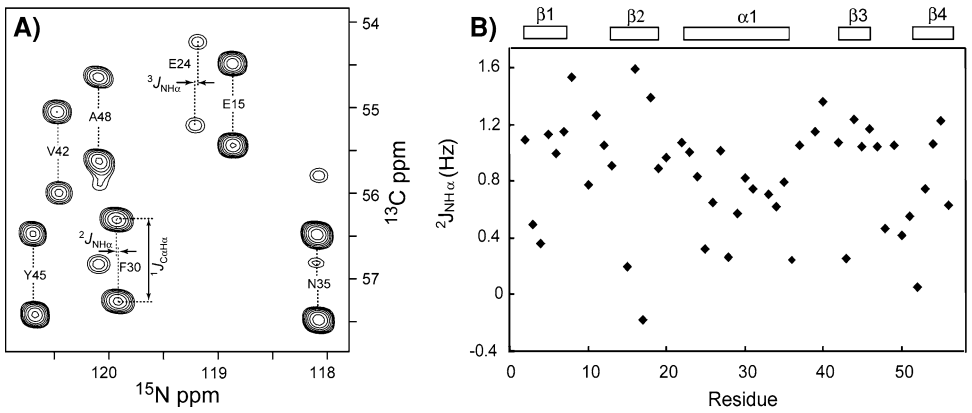

Fig. 2 Measurement of $^{2}J_{NH\alpha}$ values in the K4AK19EV42E mutant of GB3. (**a**) Superimposed regions of six ^{15}N–$^{13}C^{\alpha}$ cross-sections taken through the 3D HNCA[HA] E.COSY spectrum. The spectrum has been recorded at high resolution in the ^{15}N dimension, such as to enhance the precision at which the $^{2}J_{NH\alpha}$ (and $^{3}J_{NH\alpha}$) can be measured. The pulse sequence used for generating this spectrum is available as Supplementary Material. The intense correlations correspond to intraresidue connectivities; the weaker correlations (e.g., E24) correspond to sequential connectivities to $^{13}C^{\alpha}$ of the preceding residue. (**b**) $^{2}J_{HNC\alpha}$ values as a function of residue number. Error in the measurement is estimated at $\pm$ 0.2 Hz

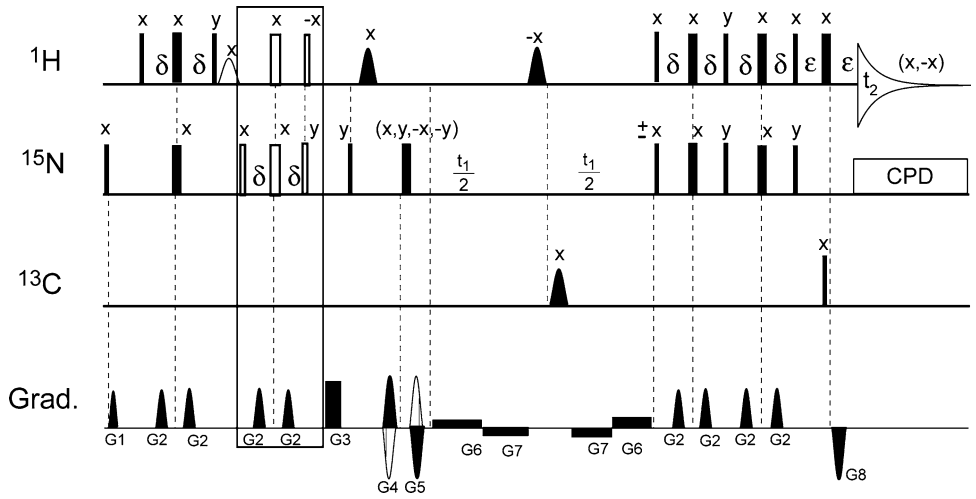

Fig. 3 Pulse scheme of the gradient-enhanced 2D BSD-IPAP HSQC experiment. The pulses in the box are only applied for generating the antiphase (AP) spectrum and are omitted for generating the in-phase (IP) spectrum. Narrow and wide pulses correspond to 90° and 180° flip angles respectively. The ^{1}H 90° water flip back pulse is sine-bell shaped, has a duration of 1.5 ms, and is only applied for the IP experiment. Solid shaped ^{1}H pulses are of the IBURP2 type (Geen and Freeman 1991) and serve to decouple $H^{\alpha,\beta}$ from ^{15}N. They are centered at 2.4 ppm, with a duration adjusted to invert ± 2.8 ppm. A 600 μs 180° hyperbolic secant shaped pulse (Silver et al. 1984), centered at 116 ppm, is used to decouple C^{α} and C′. Rance-Kay t_1 quadrature detection is used by alternating the phase of the ^{15}N 90° pulse after G_6 between x and $-x$, in concert with alternating the polarity of G_4 and G_5 (Kay et al. 1992). Pulsed field gradients $G_{1,2,4,5,8}$ are sine-bell shaped 6.6 (G_1), 9.0 (G_2), 28.2 (G_4), −28.2 (G_5) and 28.2 (G_8) G/cm. G_3, G_6 and G_7 are rectangular with strengths of 16.2 (G_3), 0.6 (G_6) and −0.6 (G_7) G/cm. Gradient durations: $G_{1,2,3,4,5,6,7,8}$ = 1.9, 2.65, 1.7, 1.0, 1.0, t_1/4, t_1/4, 0.203 ms. Delay durations: δ = 2.65 ms; ε = 0.55 ms. A more balanced way of recording IPAP spectra can be achieved by reducing the relaxation difference between IP and AP, executing both IP and AP spectra with the boxed region of Fig. 3 in place, but inserting ^{1}H 180° pulses at the center of each δ delay (and removal of the 180 ^{1}H pulse applied between the two δ delays, see Supplementary Figure S2 for details)

spectra, e.g. executing both IP and AP spectra with the boxed region of Fig. 3 in place, but inserting ^{1}H 180° pulses at the center of each δ delay (and removal of the 180 ^{1}H pulse applied between the two δ delays, see Fig. S2 for details). Relative scaling of the two spectra prior to addition/subtraction nevertheless remains necessary as for the AP spectra ^{15}N magnetization on average is more in-phase than for the IP spectrum, making it less sensitive to ^{1}H spin flips during 2δ. The IPAP-HSQC experiment of Ottiger et al. (1998a) does not include gradient-enhanced detection or active water flip-back, causing the spin state of $^{1}H^{\alpha}$ and other protons to be "scrambled" by the reverse-INEPT scheme which separates ^{15}N evolution and $^{1}H^{N}$ detection. If, instead, a gradient-enhanced conversion scheme is used to transfer ^{15}N magnetization back to $^{1}H^{N}$ (Kay et al. 1992), the spin state of protons not attached to ^{15}N to first order (neglecting relaxation during the transfer scheme) remains unchanged, and an E.COSY type fine structure can be seen in the ^{1}H–^{15}N correlations. This fine structure (Fig. 1c) results from protons that have a non-zero $^{3}J_{HH}$ or RDC interaction to $^{1}H^{N}$ and a $^{n}J_{HN}$ or RDC interaction to ^{15}N. Although, to first order, the unresolved fine structure in the upfield and downfield ^{15}N–{^{1}H} doublet components is the same, thereby not impacting the ^{15}N–^{1}H splitting derived from such spectra, in practice the line widths of the two $^{1}J_{NH}$ doublet components differ in the ^{15}N dimension due to interference between the ^{15}N–^{1}H dipolar and ^{15}N CSA relaxation mechanisms (Goldman 1984). This difference in line width, combined with the presence of (unresolved) fine structure, can give rise to problems when using peak fitting software to determine the center of each ^{15}N–{$^{1}H^{N}$} doublet component, thereby adversely impacting the accuracy at which $^{1}J_{NH}$ splittings can be measured.

Band-selective ^{1}H decoupling of the aliphatic protons during the t_1 evolution period provides an easy solution to remove the fine structure in the ^{15}N dimension of the spectrum. In principle, this could be accomplished by application of a single band-selective ^{1}H inversion pulse at the mid-point of t_1 evolution. However, during the application of such a pulse, the ^{15}N dephasing caused by the $^{1}J_{NH}$ coupling is scaled down. This $^{1}J_{NH}$ scaling during the pulse results from $^{1}H^{N}$ nutation about an effective field that deviates from the z axis, impacting $^{1}J_{NH}$ dephasing in the same manner as does off-resonance decoupling. For this reason, the decoupling is accomplished by the application of two band-selective IBURP pulses: one preceding and one following the 180° ^{15}N pulse that is already present for gradient encoding. In this manner, the effect of evolution during the application of the IBURP pulses is fully refocused, and ^{15}N–{$^{1}H^{N}$} doublets can be phased to pure absorption.

Optimal sensitivity can be obtained when the water signal is actively restored to the z axis during the execution of the pulse sequence (Grzesiek and Bax 1993). Weak gradients of opposite phase are used during t_1 evolution, such that the water signal which is inverted during the first IBURP pulse is not subject to radiation damping, and the second IBURP pulse then returns it to the $+z$ axis. As mentioned above, the gradient-enhanced readout sequence, following t_1, yields zero net rotation for proton spins not directly attached to ^{15}N, and therefore leaves the water along the $+z$ axis. Prior to t_1 evolution, the water-flip back feature is accomplished in slightly different ways for the in-phase and anti-phase versions of the experiment: For the in-phase experiment, where t_1 evolution immediately follows the initial ^{1}H $\rightarrow$ ^{15}N INEPT magnetization transfer, a 90° water-selective pulse is applied to restore water magnetization to $+z$; for the antiphase experiment, the water magnetization is flipped back to the $+z$ axis by the non-selective ^{1}H 90°$_{-x}$ purge pulse, applied just prior to ^{15}N evolution (Fig. 3).

The above described band-selective inversion pulses remove the net t_1 evolution of $J_{\mathrm{N-HR}}$ couplings, and thereby the unresolved fine structure and associated line shape asymmetry from the ^{15}N dimension. It is interesting to note that cross-correlated relaxation affects QJ experiments in the same manner as the IPAP-HSQC experiment described here, and the same solution to removal of these effects in such QJ experiments has been described previously by de Alba and Tjandra (de Alba and Tjandra 2006b). Whereas the E.COSY effects do not impact the QJ experiments, we find that the systematic errors in the $^1J_{\mathrm{NH}}$ splitting measurement resulting from them for the gradient-enhanced IPAP-HSQC experiments are comparable to those resulting from cross-correlated relaxation.

Application to GB3

Two-dimensional gradient-enhanced ^{15}N–^{1}H IPAP-HSQC spectra, in the absence and presence of band-selective-decoupling during t_1 evolution, were recorded for mutants of GB3, developed previously to alter GB3's alignment in liquid crystalline Pf1 (Yao and Bax 2007). As can be seen for a small expanded region of such a spectrum recorded under isotropic conditions (Fig. 4a), in the absence of band-selective-decoupling several of the correlations show a small tilt, marked by arrows, resulting from E.COSY effects involving $^3J_{\mathrm{HNH}\alpha}$ and $^2J_{\mathrm{NH}\alpha}$. This tilt disappears when band-selective-decoupling is used (Fig. 4b). For weakly aligned samples recorded in the presence of Pf1, the effect tends to be more pronounced as the RDCs can be considerably larger than $^3J_{\mathrm{HNH}\alpha}$ and $^2J_{\mathrm{NH}\alpha}$ (Fig. 4c) but it again disappears upon the use of band-selective decoupling (Fig. 4d). Comparison of the $^1J_{\mathrm{NH}}$ splittings extracted for the isotropic protonated sample with those obtained for perdeuterated ^{13}C/^{15}N– enriched protein (where experiments with and without band-selective decoupling yield

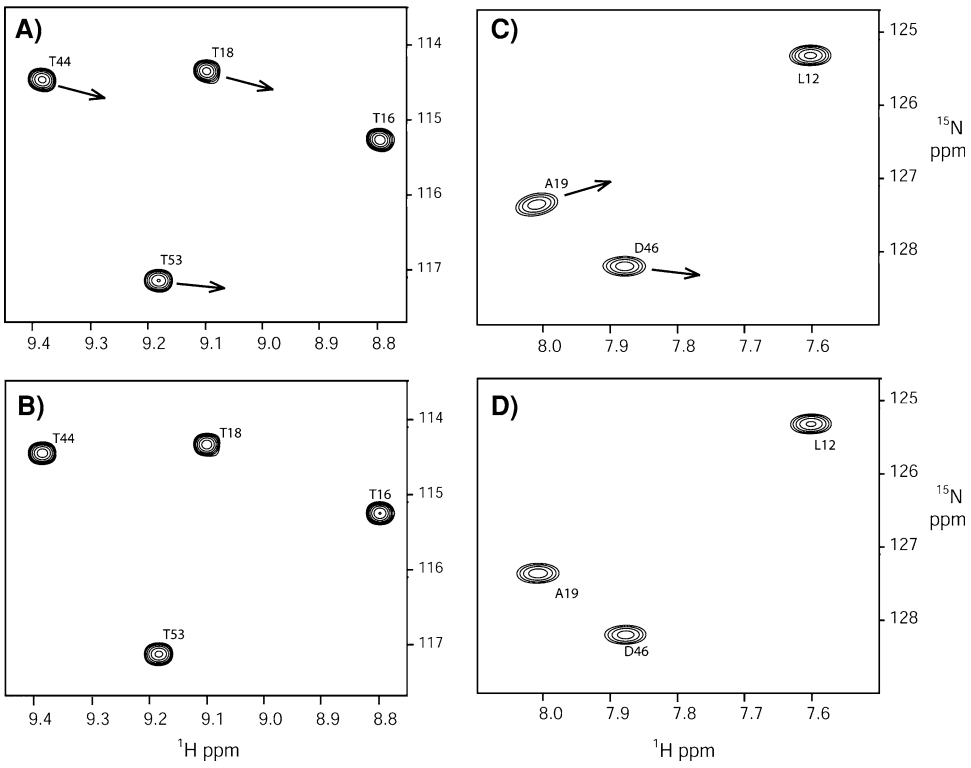

Fig. 4 Small regions extracted from the IPAP-HSQC spectra, displaying the downfield doublet components for a small spectral region of (**a**, **b**) isotropic and (**c**, **d**) Pf1-aligned GB3. (**a**, **c**) Recorded in the absence and (**b**, **d**) in the presence of band-selective ^{1}H decoupling during t_1. The arrows indicate the skewing of the cross peak shape resulting from unresolved E.COSY patterns (see main text and Fig. 1c)

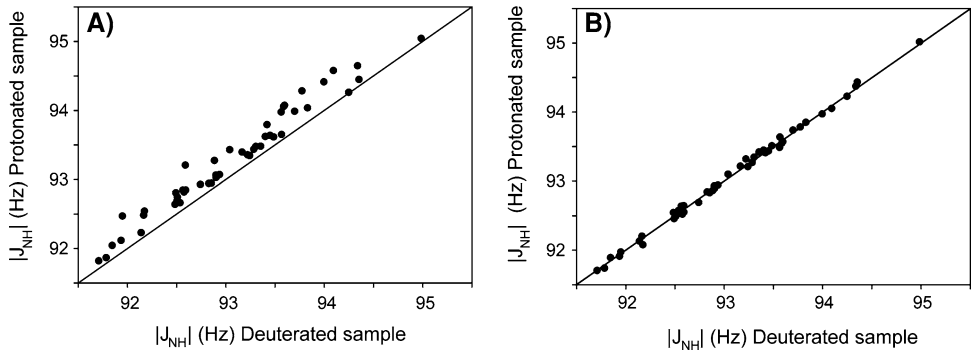

Fig. 5 Comparison of backbone $^{1}J_{NH}$ splittings measured for the U{^{1}H,^{13}C,^{15}N} and U{^{2}H,^{13}C,^{15}N} K4AK19EV42E mutant of GB3. $^{1}J_{NH}$ splittings measured for the protonated and deuterated samples using the gradient-enhanced IPAP-HSQC experiment **a** in the absence and **b** in the presence of band-selective decoupling. The measurements were performed at 750 MHz ^{1}H frequency

values that are within experimental uncertainty from one another) shows excellent agreement when band-selective decoupling is used (Fig. 5b) but considerable scatter and a systematic offset in the absence of band-selective decoupling (Fig. 5a).

The observation that the $^{1}J_{NH}$ splitting in the absence of band-selective decoupling is systematically larger results from the above described cross-correlated relaxation effect: The $^{3}J_{NH\beta}$ coupling is negative (taking into account the negative sign of γ_N), as is the value of $P_2(\cos\theta)$. For $^{2}J_{NH\alpha}$, the sign of the coupling is positive (Fig. 2) but so is its $P_2(\cos\theta)$ (for the common case where the backbone torsion angle φ falls between $-153°$ (T18) and $-64°$ (K10)). Therefore, in both cases the outer multiplet components in the diagram of Fig. 1b are sharper and slightly more intense than the inner components, giving rise to the small increase in the magnitude of the apparent splitting. When line broadening is applied in the ^{15}N dimension, which decreases the asymmetry in the line shapes of each of the doublet components, the difference in splitting relative to measurements on the perdeuterated protein decreases, but so does the precision of the measurement (data not shown).

High quality of the values of the $^{1}J_{NH}$ couplings obtained with band-selective decoupling on protonated samples is also demonstrated by fitting the difference in $^{1}J_{NH}$ measured at 750 and 500 MHz ^{1}H frequencies to the structure of GB3. The difference in $^{1}J_{NH}$ results from two contributions: a dynamic frequency shift (Tjandra et al. 1996; Werbelow 1996; de Alba and Tjandra 2006b) and residual dipolar coupling, caused by the weak alignment of the protein induced by anisotropy of its magnetic susceptibility (Gayathri et al. 1982; Tolman et al. 1995; Tjandra et al. 1996). Even while the differences in RDC at 500 and 750 MHz are extremely small, they agree well with the structure of the protein (Fig. 6). The best fit, shown in Fig. 6, includes a uniform +0.106 Hz contribution from the dynamic frequency shift, which is in excellent agreement with a theoretical value of 0.102 Hz, expected for a

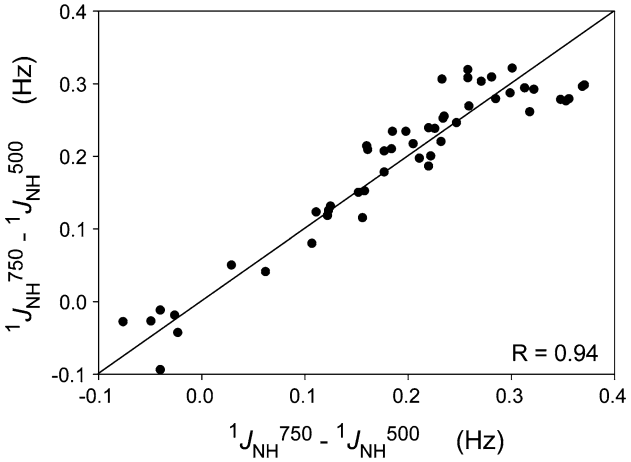

Fig. 6 Correlation between experimental (x axis) and predicted magnetic field dependence of the $^{1}J_{NH}$ splittings in GB3. The predicted values are obtained from an SVD fit of differences between $^{1}J_{NH}$ splittings measured at 750 and 500 MHz ^{1}H frequencies to the N–H vector orientations of GB3 (Yao et al. 2008b), with the dynamic frequency shift treated as a variable which is assumed to be uniform across all amides. The fitted alignment tensor amplitude (D_a) is -0.121 Hz, the rhombicity is 0.576 and the three Euler angles are 18°, 314°, 117° (z-y-z convention) relative to the frame of the PDB coordinates (entry 2OED). The fitted dynamic frequency shift equals 0.106 Hz, in good agreement with an expected value of 0.102 Hz, calculated for $\tau_c = 3.3$ ns (Hall and Fushman 2003)when neglecting internal dynamics and using the constants and approximations of Tjandra et al. (1996). The root mean square deviation (RMSD) between the experimental and best-fitted $^{1}J_{NH}^{750}-{}^{1}J_{NH}^{500}$ values is 0.037 Hz

rigid protein diffusing isotropically with a rotational correlation time of 3.3 ns (Hall and Fushman 2003).

To test the performance of regular IPAP and BSD-IPAP HSQC on an aligned sample, we measured the RDCs of aligned protonated U[^{15}N,^{13}C] mutant GB3 K19AV42ED47K ($D_a = 12.0$ Hz). By fitting the RDCs to the structure previously determined on the basis of six sets of RDCs, measured under different alignments on perdeuterated proteins, the BSD-IPAP determined RDCs yield

an rmsd of 0.29 Hz while the regular IPAP RDCs yield 0.33 Hz. The improvement is only moderate, and the low rmsd indicates that the error in measuring the $^1J_{NH}$ splitting partly cancels when calculating the RDC from the difference in such splittings. However, it is also worth noting that the RDCs measured on deuterated proteins, and used to refine the structure, yield an rmsd of 0.22 Hz ($D_a = 10$ Hz), suggesting that structural noise in part obscures the improved accuracy of the BSD-IPAP RDCs.

Concluding remarks

The precision of NMR measurements, as defined by their random error or reproducibility when repeating the same measurement, provides only a lower limit for the true uncertainty in the measurement. Especially in cases where systematic errors can occur, such as demonstrated above for $^1J_{NH}$ measurement on protonated proteins where cross-correlated relaxation and unresolved E.COSY effects can perturb the measured couplings, the true uncertainty can be considerably larger than the random error. For our $^1J_{NH}$ measurements in GB3, the systematic errors resulting from cross-correlated relaxation and E.COSY effects are at most a few tenths of a Hertz, i.e., nearly two orders of magnitude smaller than the RDC values measured in Pf1. When using such couplings for the purpose of structure determination or refinement, the impact of these errors tends to be negligible. For example, 2° of structural noise causes root-mean-square changes in predicted couplings that are about 7% of the applicable dipolar coupling strength, D_a (Zweckstetter and Bax 2002). This therefore means that for aligned proteins, with $|D_a|$ values greater than $\sim$5 Hz, the measurement errors are of the same order as the impact on RDCs of changes in bond vector orientations by at most a few degrees, smaller than the errors made by common assumptions such as planarity of peptide groups. For most practical purposes, these measurement errors therefore have negligible impact during structure calculation. On the other hand, when interpreting inconsistencies between measurements made under different alignment conditions in terms of dynamics (Peti et al. 2002; Tolman 2002; Bruschweiler 2003; Hus et al. 2003; Bouvignies et al. 2005; Bouvignies et al. 2006; Lakomek et al. 2006; Tolman and Ruan 2006; Lakomek et al. 2008; Lange et al. 2008; Yao et al. 2008b), substantial amplitudes of internal dynamics may be required to reconcile small differences between observed RDCs and values predicted for a rigid protein. In this respect, it is interesting to note that for a recently measured set of RDCs on six perdeuterated GB3 mutants, dynamics analysis of the RDCs yielded a more homogeneous pattern of internal dynamics (Yao et al. 2008a) than for earlier measurements on the same set of protonated GB3 mutants (Yao et al. 2008b). For the perdeuterated set, RDC analysis of the internal dynamics yields a profile closely resembling that obtained from ^{15}N relaxation (Hall and Fushman 2003), except for larger amplitude motions in two loop regions (Yao et al. 2008a; Yao et al. 2008b).

Supplementary material

One figure showing the HNCA[HA] pulse diagram; Bruker code for the pulse programs used for this experiment and for the band-selective-decoupled IPAP-HSQC experiment of Fig. 3; one figure showing a modified IPAP-HSQC experiment and corresponding Bruker code; one table with the $^2J_{NH\alpha}$ couplings measured in the K4AK19EV42E GB3 mutant; one table with the $^1J_{NH}$ splittings measured for the protonated protein at 500 and 750 MHz.

Acknowledgment This work was supported in part by the Intramural Research Program of the NIDDK, NIH, and by the Intramural AIDS-Targeted Antiviral Program of the Office of the Director, NIH.

References

Archer SJ, Ikura M, Torchia DA, Bax A (1991) An alternative 3D NMR technique for correlating backbone ^{15}N with sidechain H^{β} resonances in larger proteins. J Magn Reson 95:636–641

Bouvignies G, Bernado P, Meier S, Cho K, Grzesiek S, Bruschweiler R, Blackledge M (2005) Identification of slow correlated motions in proteins using residual dipolar and hydrogen-bond scalar couplings. Proc Natl Acad Sci U S A 102:13885–13890

Bouvignies G, Markwick P, Brueschweiler R, Blackledge M (2006) Simultaneous determination of protein backbone structure and dynamics from residual dipolar couplings. J Am Chem Soc 128:15100–15101

Bruschweiler R (2003) New approaches to the dynamic interpretation and prediction of NMR relaxation data from proteins. Curr Opin Struct Biol 13:175–183

Bystrov VF (1976) Spin–spin couplings and the conformational states of peptide systems. Prog. NMR Spectrosc 10:41–81

Cutting B, Tolman JR, Nanchen S, Bodenhausen G (2002) Accurate measurement of residual dipolar couplings in anisotropic phase. J Biomol NMR 23:195–200

de Alba E, Tjandra N (2006a) Interference between cross-correlated relaxation and the measurement of scalar and dipolar couplings by quantitative J. J Biomol NMR 35:1–16

de Alba E, Tjandra N (2006b) On the accurate measurement of amide one-bond N-15-H-1 couplings in proteins: effects of cross-correlated relaxation, selective pulses and dynamic frequency shifts. J Magn Reson 183:160–165

Delaglio F, Grzesiek S, Vuister GW, Zhu G, Pfeifer J, Bax A (1995) NMRpipe–a multidimensional spectral processing system based on unix pipes. J Biomol NMR 6:277–293

Gayathri C, Bothnerby AA, Vanzijl PCM, Maclean C (1982) Dipolar Magnetic-Field effects in NMR spectra of liquids. Chem Phys Lett 87:192–196

Geen H, Freeman R (1991) Band-selective radiofrequency pulses. J Magn Reson 93:93–141

Goldman M (1984) Interference effects in the relaxation of a pair of unlike spin-1/2 nuclei. J Magn Reson 60:437–452

Griesinger C, Sorensen OW, Ernst RR (1985) Two-dimensional correlation of connected NMR transitions. J Am Chem Soc 107:6394–6396

Griesinger C, Sørensen OW, Ernst RR (1986) Correlation of connected transitions by two-dimensional NMR spectroscopy. J Chem Phys 85:6837–6852

Grzesiek S, Bax A (1993) The importance of not saturating H_2O in protein NMR. Application to sensitivity enhancement and NOE measurement. J Am Chem Soc 115:12593–12594

Hall JB, Fushman D (2003) Characterization of the overall and local dynamics of a protein with intermediate rotational anisotropy: differentiating between conformational exchange and anisotropic diffusion in the B3 domain of protein G. J Biomol NMR 27: 261–275

Hansen MR, Mueller L, Pardi A (1998) Tunable alignment of macromolecules by filamentous phage yields dipolar coupling interactions. Nat Struct Biol 5:1065–1074

Hus JC, Peti W, Griesinger C, Bruschweiler R (2003) Self-consistency analysis of dipolar couplings in multiple alignments of ubiquitin. J Am Chem Soc 125:5596–5597

Kay LE, Keifer P, Saarinen T (1992) Pure absorption gradient enhanced heteronuclear single quantum correlation spectroscopy with improved sensitivity. J Am Chem Soc 114:10663–10665

Lakomek NA, Carlomagno T, Becker S, Griesinger C, Meiler J (2006) A thorough dynamic interpretation of residual dipolar couplings in ubiquitin. J Biomol NMR 34:101–115

Lakomek NA, Walter KFA, Fares C, Lange OF, de Groot BL, Grubmuller H, Bruschweiler R, Munk A, Becker S, Meiler J, Griesinger C (2008) Self-consistent residual dipolar coupling based model-free analysis for the robust determination of nanosecond to microsecond protein dynamics. J Biomol NMR 41:139–155

Lange OF, Lakomek NA, Fares C, Schroder GF, Walter KFA, Becker S, Meiler J, Grubmuller H, Griesinger C, de Groot BL (2008) Recognition dynamics up to microseconds revealed from an RDC-derived ubiquitin ensemble in solution. Science 320:1471–1475

Meissner A, Schulte-Herbruggen T, Sorensen OW (1998) Spin-state-selective polarization or excitation for simultaneous E. COSY-type measurement of 3J(C′, Ha) coupling constants with enhanced sensitivity and resolution in multidimensional NMR spectroscopy of 13C, 15N– labeled proteins. Journal of American Chemical Society 120:3803–3804

Montelione GT, Wagner G (1989) Accurate measurements of homonuclear HN–Ha coupling constants in polypeptides using heteronuclear 2d NMR experiments. J Am Chem Soc 111:5474–5475

Ottiger M, Delaglio F, Bax A (1998a) Measurement of J and dipolar couplings from simplified two-dimensional NMR spectra. J Magn Reson 131:373–378

Ottiger M, Delaglio F, Marquardt JL, Tjandra N, Bax A (1998b) Measurement of dipolar couplings for methylene and methyl sites in weakly oriented macromolecules and their use in structure determination. J Magn Reson 134:365–369

Peti W, Meiler J, Bruschweiler R, Griesinger C (2002) Model-free analysis of protein backbone motion from residual dipolar couplings. J Am Chem Soc 124:5822–5833

Prestegard JH, Al-Hashimi HM, Tolman JR (2000) NMR structures of biomolecules using field oriented media and residual dipolar couplings. Q Rev Biophys 33:371–424

Silver MS, Joseph RI, Hoult DI (1984) Highly selective Pi/2 and Pi-pulse generation. J Magn Reson 59:347–351

Tjandra N, Bax A (1997) Measurement of dipolar contributions to 1JCH splittings from magnetic-field dependence of J modulation in two-dimensional NMR spectra. J Magn Reson 124:512–515

Tjandra N, Grzesiek S, Bax A (1996) Magnetic field dependence of nitrogen-proton J splittings in N– 15– enriched human ubiquitin resulting from relaxation interference and residual dipolar coupling. J Am Chem Soc 118:6264–6272

Tjandra N, Omichinski JG, Gronenborn AM, Clore GM, Bax A (1997) Use of dipolar 1H–15N and 1H–13C couplings in the structure determination of magnetically oriented macromolecules in solution. Nat Struct Biol 4:732–738

Tolman JR (2002) A novel approach to the retrieval of structural and dynamic information from residual dipolar couplings using several oriented media in biomolecular NMR spectroscopy. J Am Chem Soc 124:12020–12030

Tolman JR, Ruan K (2006) NMR residual dipolar couplings as probes of biomolecular dynamics. Chem Rev 106:1720–1736

Tolman JR, Flanagan JM, Kennedy MA, Prestegard JH (1995) Nuclear Magnetic Dipole interactions in field-oriented proteins—information for structure determination in solution. Proc Natl Acad Sci U S A 92:9279–9283

Wagner G, Schmieder P, Thanabal V (1991) A new 1H–15N–13C triple resonance experiment for sequential assignments and measuring homonuclear Halpha-HN coupling constants in polypeptides. J Magn Reson 93:436–440

Wang AC, Bax A (1995) Reparametrization of the Karplus relation for (3)J(H-Alpha-N) and (3)J(H-N-C′) in peptides from uniformly C-13/N-15-enriched human ubiquitin. J Am Chem Soc 117:1810–1813

Wang AC, Bax A (1996) Determination of the backbone dihedral angles phi in human ubiquitin from reparametrized empirical Karplus equations. J Am Chem Soc 118:2483–2494

Werbelow LG (1996) The dynamic frequency shift. In: Grant DM, Harris RK (eds) Encyclopedia of nuclear magnetic resonance, vol 6. Wiley, London, pp 4072–4078

Yang DW, Nagayama K (1996) A sensitivity-enhanced method for measuring heteronuclear long-range coupling constants from the displacement of signals in two 1D subspectra. J Magn Reson Ser A 118:117–121

Yao LS, Bax A (2007) Modulating protein alignment in a liquid-crystalline medium through conservative mutagenesis. J Am Chem Soc 129:11326–11327

Yao L, Voegeli B, Ying JF, Bax A (2008a) NMR determination of amide N–H equilibrium bond length from concerted dipolar coupling measurements. J Am Chem Soc 130:16518–16520

Yao L, Vogeli B, Torchia DA, Bax A (2008b) Simultaneous NMR study of protein structure and dynamics using conservative mutagenesis. J Phys Chem B 112:6045–6056

Ying JF, Chill JH, Louis JM, Bax A (2007) Mixed-time parallel evolution in multiple quantum NMR experiments: sensitivity and resolution enhancement in heteronuclear NMR. J Biomol NMR 37:195–204

Zweckstetter M, Bax A (2002) Evaluation of uncertainty in alignment tensors obtained from dipolar couplings. J Biomol NMR 23: 127–137